**Proceedings of the ASME 2018**
**Pressure Vessels and Piping Conference**
**PVP2018**
**July 15-20, 2018, Prague, Czech Republic**

**PVP2018-84427**

# CONSTRAINT ASSESSMENT FOR CRUCIFORM SPECIMENS WITH A SEMI-ELLIPTICAL CRACK

**Yupeng Cao**
Department of Component Research and Design,
Shanghai Nuclear Engineering Research and Design Institute,
Shanghai 200237, China
Email: caoyupeng@snerdi.com.cn

**Guian Qian** [1]
State Key Laboratory for Nonlinear Mechanics (LNM), Institute of Mechanics, Chinese Academy of Sciences, Beijing 100190, China
Email: qianguian@imech.ac.cn

**Yinbiao He**
Department of Component Research and Design,
Shanghai Nuclear Engineering Research and Design Institute,
Shanghai 200237, China
Email: hybly@snerdi.com.cn

**Yuh J Chao**
Department of Mechanical Engineering,
University of South Carolina, Columbia, SC 29208, USA
Email: CHAO@sc.edu

## ABSTRACT

A real crack to be assessed in a RPV is generally a shallow crack subjected to biaxial far-field stresses. However, the fracture toughness $K_c$ or $J_c$, which is an important material property for the structural integrity assessment of RPV containing cracks, are usually tested on deep cracked compact tension [C(T)] or single-edged bending [SE(B)] specimens under uniaxial loading. The fracture toughness data do not reflect the realistic biaxial loading state that the cracks are subjected to. Cruciform bending [CR(B)] specimen is therefore developed to simulate the biaxial stress state. In this paper, a series of finite element (FE) simulations of the CR(B) specimens containing different semi-elliptical cracks are conducted. Stress-strain curves of materials of different yield strength and hardening behavior reflecting the variation in the mechanical properties of RPV steels due to aging or temperature change are implemented into the finite element models. The $J$-$A_2$ theory is applied to analyze the crack tip constraint. The results show that the biaxial effect is material property dependent and affected by load levels.

## INTRODUCTION

Generally, a real flaw detected during in-service inspections of the reactor pressure vessel (RPV) of a nuclear power plant is a shallow crack or an embedded crack, which is subjected to combined thermal-mechanical loads, such as normal operational pressure temperature (P-T) transients and pressurized thermal shock (PTS) upset transients. The thermal, pressure and residual stresses in the RPV wall are combined to form a biaxial stress state at the crack tip as schematically shown in Fig. 1, where $t$ is the thickness of the RPV wall. However, the fracture toughness of materials, $K_c$ or $J_c$, required for the structural integrity assessment is obtained on the conventional deep cracked SE(B) and C(T) specimens under uniaxial loading following the ASTM and ISO standards. The crack tip stress state in the specimens is quite different from that of a real crack in RPV.

Therefore, a special cruciform bend specimen [CR(B)] was first developed by the HSST Program at ORNL to introduce an in-plane and out-of-plane biaxial stress field that approximates the biaxial stresses resulted from P-T or PTS loading, which is used to address the influence of biaxial stress effects on fracture. The CR(B) specimen enables controlled biaxial loading ratios for cracks by the choice of appropriate span width ratios of the longitudinal beam arms to the transverse beam arms.

Most studies concerning the biaxial loading effect involve the CR(B) specimens with a straight-fronted crack. A series of large (100×100 mm cross-section, 4T) specimen of this type made of an A533B steel have first been tested by Bass et al [1]. Joyce et al. [2] developed a medium scale CR(B) specimens (50×50 mm cross-section, 2T) design and performed the tests on an A533B steel. More recently, Jörg et al. [3] showed that the major effects observed in large scale CR(B) specimen could

[1] Laboratory for Nuclear Materials, Paul Scherrer Institute

be reproduced in the small-scale CR(B) specimen (10×20 mm cross-section). Numerical study by Sharp and Chao [4] showed that the biaxial effect as seen from the tests on the CR(B) specimens can be predicted by the $J$-$A_2$ theory.

Some investigations use the CR(B) specimens containing a shallow semi-elliptical surface flaw, considering a real surface crack shape is generally idealized as a semi-ellipse. The CR(B) containing this type of flaw may exhibit the different trends of biaxial effect as observed in the specimens with straight-fronted cracks due to different crack shapes. The biaxial bend cruciform tests of semi-elliptical cracks in a RPV longitudinal weld were conducted with the NESC-IV project to address the transferability of fracture toughness data from laboratory specimens to cracks in RPV applications [5]. Further work on evaluation of the influence of warm pre-stress on surface cracks in RPVs for NESC-VII project conducted experiments on the 18MND5 CR(B) specimens with semi-elliptical cracks [6].

Our paper PVP2017-65979 conducted the constraint analysis of CR(B) specimens with a straight-front shallow crack, showing the evolution of the biaxial effect with the various material tensile properties and the crack depths [7]. This paper expands on our previous research, aiming in evaluation of biaxial effect on the surface-breaking flaws in CR(B) specimens by using the $J$-$A_2$ methodology.

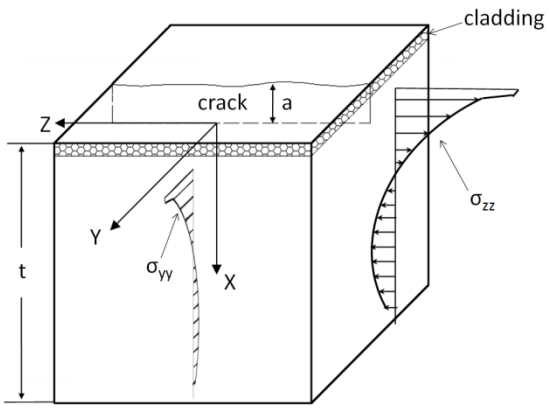


**Figure 1 Biaxial stress state of the crack in RPV wall under PTS transients**

## NOMENCLATURE

| | |
|---|---|
| $\sigma_0$ | yield stress |
| $\varepsilon_0$ | strain parameter in the Ramberg–Osgood stress–strain relationship |
| $\alpha$ | parameter in the Ramberg-Osgood stress–strain relationship |
| $n$ | hardening exponent in the Ramberg–Osgood stress–strain relationship |
| $E$ | elastic modulus |
| $v$ | Poisson's ratio |
| $A_2$ | constraint parameter in the $J$-$A_2$ theory |
| $s_1$, $s_2$, $s_3$ | stress power exponents in the $J$-$A_2$theory |
| $\tilde{\sigma}_{ij}^{(k)}(\theta,n)$ | dimensionless stress functions in the $J$-$A_2$ theory |
| $I_n$ | an integration constant |
| $L$ | a characteristic length parameter |
| $K_c$ | material fracture toughness |
| $J$ | $J$-integral |
| $J_c$ | critical $J$-integral |
| $S_1$, $S_2$ | span widths on the longitudinal and the transverse beam arms |
| $W$ | specimen width |
| $B$ | specimen thickness or crack front lengths |
| $a_0$ | initial crack depth |
| $T_0$ | Master curve reference temperature |
| $\Phi$ | angle |

## $J$-$A_2$ METHODOLOGY

The uniaxial tensile property of the material represented by the Ramberg-Osgood stress–strain relationship has the form

$$\frac{\varepsilon}{\varepsilon_0}=\frac{\sigma}{\sigma_0}+\alpha\left(\frac{\sigma}{\sigma_0}\right)^n \tag{1}$$

where $\sigma_0$ and $\varepsilon_0=\sigma_0/E$ can be taken as the yield stress and the yield strain, respectively; $E$ is Young's modulus; $\alpha$ is a material constant and $n$ is the strain hardening exponent.

The stress fields at a crack tip in a power-law plasticity material such as the Ramberg-Osgood material in Eq.(1) may be characterized by the classical HRR solution[8-10] from fracture mechanics theory as

$$\sigma_{ij}=\sigma_0\left(\frac{J}{\alpha\varepsilon_0\sigma_0 I_n r}\right)^{1/n+1}\tilde{\sigma}_{ij}(\theta,n) \tag{2}$$

where $I_n$ is an integration constant that depends on $n$; $i$ and $j$ represent $r$ and $\theta$ in a polar coordinate system with origin at the crack tip, and $\tilde{\sigma}_{ij}(\theta,n)$ is the dimensionless stress function of $n$ and $\theta$.

It is well known that the HRR solution can be used to characterize the stress fields only under small scale yielding (SSY) condition and high constraint specimen geometry such as the deeply-cracked C(T) and SE(B) specimens according to the ASTM test standard [11]. The crack tip stresses in the low constraint geometry generally deviate from the HRR solution gradually as the load increases. In order to solve this problem, Yang et al.[12, 13] and Chao et al. [14] developed the asymptotic solutions near a crack tip, which includes several higher order terms. It was demonstrated that the stress, strain and displacement fields in either high or low constraint specimen geometry can be well characterized by the analytical solution with only three terms, which can be written as

$$\frac{\sigma_{ij}}{\sigma_0}=A_1\left[\left(\frac{r}{L}\right)^{s_1}\tilde{\sigma}_{ij}^{(1)}(\theta,n)+A_2\left(\frac{r}{L}\right)^{s_2}\tilde{\sigma}_{ij}^{(2)}(\theta,n)+A_2^{\,2}\left(\frac{r}{L}\right)^{s_3}\tilde{\sigma}_{ij}^{(3)}(\theta,n)\right] \tag{3}$$

where the angular functions $\tilde{\sigma}_{ij}^{(k)}(\theta,n)$ (k=1, 2, 3) are the dimensionless functions of $n$ and $\theta$, the stress power exponents $s_1$, $s_2$, $s_3$ ($s_1<s_2<s_3$) are only dependent of the

hardening exponent $n$, $s_1 = -\frac{1}{n+1}$ and $s_3=2s_2-s_1$ for $n>3$. $L$ is a characteristic length parameter which can be chosen as the crack length $a$, specimen thickness $W$, or a unit length (e.g., 1 mm). The parameters $A_1$ is given by

$$A_1 = \left(\frac{J}{\alpha\varepsilon_0\sigma_0 I_n L}\right)^{-s_1} \tag{4}$$

$A_2$ is an undetermined parameter and is a function of the geometry of the specimen and the loading. Hence, $A_2$ can be used as a quantitative measure of the constraint effect. The numerical values of the parameters $\tilde{\sigma}_{ij}^{(k)}(\theta,n)$, $I_n$ and $S_k$ in Eq.(3) and Eq.(4) have been tabulated by Chao and Zhang [15].

For convenience, the parameters required for the application of the $J$-$A_2$ theory were fitted by Wang et al.[16]. The stress power exponents $s_2$ and $s_3$ are:

$$\begin{cases} s_2(n) = -0.888e^{-0.7803n} + 0.0725 & (3 \leqq n \leqq 9) \\ s_2(n) = 0.079e^{-0.0372n} + 0.0152 & (9 \leqq n \leqq 50) \end{cases} \tag{5}$$

$$s_3(n) = 2S_2(n) - s_1(n) \qquad (3 \leqq n \leqq 50) \tag{6}$$

The equations for the angular functions $\tilde{\sigma}_{ij}^{(k)}(\theta,n)$ at $\theta$= 0 and the integration constant $I_n$ are fitted as follows:

$$\tilde{\sigma}_{ij}^{(1)}(\theta=0,n) = -1.217e^{-0.3867n} - 0.640e^{-0.0680n} + 2.8473 \qquad (3 \leqq n \leqq 50) \tag{7}$$

$$\tilde{\sigma}_{ij}^{(2)}(\theta=0,n) = -0.04270 + 0.2117n - 0.04659n^2 + 0.004605n^3 - 0.0001729n^4 \qquad (3 \leqq n \leqq 8) \tag{8}$$

$$\tilde{\sigma}_{\theta\theta}^{(2)}(\theta=0,n) = 0.14361e^{-0.03147n} + 0.20774 \qquad (8 \leqq n \leqq 50)$$

$$\tilde{\sigma}_{ij}^{(3)}(\theta=0,n) = 10.45624e^{-0.33465n} - 17.9685e^{0.013078n} + 13.78619 \qquad (3 \leqq n \leqq 50) \tag{9}$$

$$I_n = 1.11366e^{-0.0625n} + 2.16658e^{-0.3900n} + 3.91467 \tag{10}$$

In this study, the $J$-$A_2$ method is used to characterize the crack-tip constraints of the biaxially and uniaxially loaded CR (B) specimens containing shallow cracks with different material properties.

## FINITE ELEMENT MODEL

This study considers the specimen geometries similar to those utilized in NESC-IV project. The dimensions of the specimens are listed in Table 1 and the geometry is shown in Fig. 2. The crack depths $a_0/W$ are chosen as 0.05 and 0.1. The aspect ratio of the semi-elliptical cracks is $a_0/2c$=1:6, which is commonly specified in the standards.

**Table 1 The sizes of the specimens**

| $B$ (mm) | $W$ (mm) | $S_1$ (mm) | $S_2$ (mm) | $a_0/W$ | $a_0/2c$ |
|---|---|---|---|---|---|
| 101.6 | 101.6 | 673.2 | 673.2 | 0.05, 0.1 | 1:6 |

Two sets of the Ramberg-Osgood parameters (see Table 2 and Fig. 2) are considered to assess the influence of material tensile properties on the biaxial loading. The Poisson's ratio $v$ is assumed as 0.3. These ranges of tensile properties reflect the increase in the yield strength with the decrease in hardening exponent that are the characteristics of RPV steels due to irradiation and the variations in the stress-strain relationship with temperature. The stress-strain curves considered span the range of the mechanical behavior of interest for RPV steels.

**Table 2 The assumed Ramberg-Osgood parameters of the RPV materials**

| Material IDs | $E/\sigma_0$ | α | $E$ (MPa) | $n$ |
|---|---|---|---|---|
| 1 | 800 | 1.6 | 206000 | 5 |
| 2 | 300 | 0.6 | 206000 | 20 |

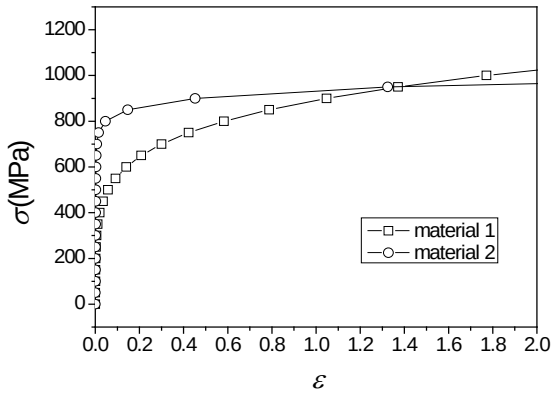


**Figure 2 The stress-strain curves**

By taking into account of symmetry, only one-quarter of the CR(B) specimens are modeled using the commercial finite element (FE) code ABAQUS [17] as shown in Fig. 3. In the numerical calculation, the CR(B) specimen model under biaxial loading is loaded by the central support with the prescribed displacement and the two rollers are fixed to ensure the equal spans as indicted in Fig. 2, where $S_1$ and $S_2$ are the spans, $W$ is the width, $a_0$ is the crack depth, and $B$ is the thickness of the specimen. The support and the rollers are modeled as the rigid bodies. The support and the rollers interact with the deformable test specimen via the frictionless contact formulation. The uniaxial loading is realized by removal of the roller interacting with transverse beam arm.

For each FE model of the specimens (the biaxial and uniaxial loaded specimens), two crack depths ($a_0/W$=0.05, $a_0/W$=0.1) are considered. The minimum element size along the

ligament ahead of the crack tip is 10 μm. In the range of 4 mm around the crack tip, the FE mesh designs are similar in all the models. The elements used are the reduced-integration linear elements (designated as C3D8R in ABAQUS). A coordinate system for the specimens is shown in Fig. 4 such that the x-axis lies in the crack plane and points to the specimen width direction; the y-axis lies in the thickness direction and the z-axis is orthogonal to the crack plane. The origin of the coordinate system is located at the center of the semi-ellipse.

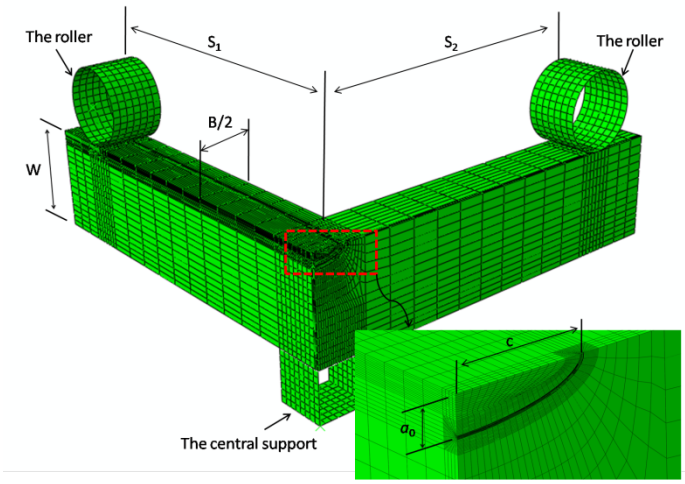


**Figure 3 Finite element meshes for the CR(B) specimen**

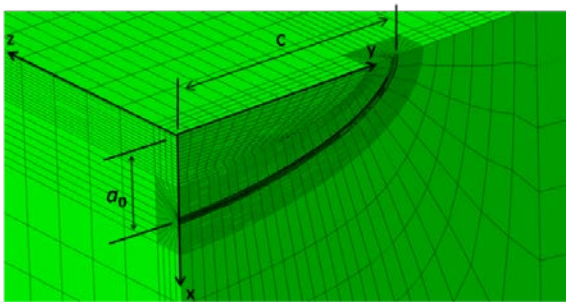


(a)

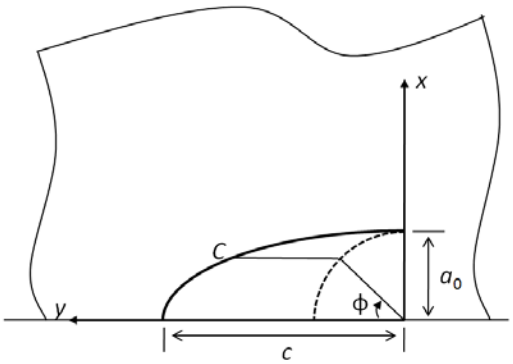


(b)

**Figure 4 Co-ordinate system for a semi-elliptical crack**

## CONSTRAINT ANALYSIS WITH *J*-$A_2$ METHOD

The constraint parameter $A_2$ in Eq. (3) is determined using a point match technique described as following:

(1) Obtain the opening stress distribution $\sigma_{\theta\theta}$ ($\sigma_{zz}$ in this study as shown in Fig. 4) at a point of interest along the crack front (e.g. *C* point in Fig. 4 (b) ) from the FE analysis.

(2) Set the $\sigma_{\theta\theta}$ from the FE analysis equal to the three-term analytical function Eq. (3) to create a quadratic equation with respect to $A_2$. The characteristic length parameter $L$ is set to be 1 mm.

(3) Solve the quadratic equation for $A_2$ at each node along the ligament (in the direction normal to the crack front).

$A_2$ values are plotted in the following sections to quantify the constraints. Similar to *T*-stress and *Q*-stress theories, the higher $A_2$ means the higher constraint, which is closer to the HRR solutions. Specifically, the $\sigma_{\theta\theta}$ values in the range of $r/(J/\sigma_0)$=2-5, $\theta$=0° are used to determine an average $A_2$ in this paper.

Figs. 5 (a) and (b) show plots at different load levels ($K_J$ values converted from *J*-integrals) for the distributions of $A_2$ along the crack front in the CR(B) specimens with $a_0/W$=0.1 under biaxial and uniaxial loading. In each figure, the same values of $K_J$ at the deepest point ($\Phi$=90°) are chosen for the two loading conditions to facilitate the comparison. It should be mentioned that since only the shallow surface cracks are considered in this paper, all the crack tips thus show negative $A_2$ due to constraint loss. For uniaxial loading condition, the highest $A_2$ value (approximately -0.257) occurs at the deepest point of the crack in the specimen with $E/\sigma_0$=300. $A_2$ decreases toward the free surface at all load levels considered as $\Phi$ decreases. $A_2$ is reduced significantly in the crack front range near the free surface, especially for the material with $E/\sigma_0$=800 in Fig. 5(b). It drops from -0.392 at $\Phi$=90° to the minimum value of -0.664 at $\Phi\approx$6° at the load level $K_J$=150MPa$\sqrt{m}$. When compared with the variation of $A_2$ along the straight crack front in SE(B) specimens reported in our previous study [7], the distributions of $A_2$ values are found to have the similar trends for the uniaxially loaded CR(B) specimen.

As for the biaxial loading condition, the biaxial effect is clearly characterized by $A_2$. The values of $A_2$ at biaxial loading are generally higher than those in uniaxial loading condition for the material with $E/\sigma_0$=800. While for the $E/\sigma_0$=300 material, under the load levels ranging from $K_J$=100 MPa$\sqrt{m}$ to $K_J$=250 MPa$\sqrt{m}$, in the range of $\Phi\approx$25° to $\Phi$=90°, the biaxially loaded crack exhibits a scatter band similar to those for uniaxial loading. But in the region close to the free surface of the specimen, for both materials investigated, $A_2$ values obtained under biaxial loading are always higher than their counterparts under uniaxial loading. In the aspect of the constraint levels along the crack front, the $A_2$ values demonstrate lower tendency to drop toward the free surface. It is worth noting here that $A_2$ values peak around $\Phi$=15° at low loads for the $E/\sigma_0$=800 material and at nearly all the loads for the $E/\sigma_0$=300 material. This phenomenon is experimentally supported by NESC-IV project. In the project, the fracture surface observations of the

CR(B) specimens show that the initiation sites are mostly found in the region from $\Phi$=16° to 30°, indicating that initiation tends to occur toward the specimen surface.

Figs. 5 (a) and (b) also compare the influence of material property variations on the crack-tip constraint for the cracks under different loading conditions. For the material with a lower stress ($E/\sigma_0$=800) in Fig. 5(a), biaxial bending increase the local constraint level at the near-surface crack front (see the region around the peak value of $A_2$ for the biaxially loaded specimen in Fig. 5) under low loads and then progressively enhance the constraints along the whole crack front as the loads increase. By contrast, biaxial loading has less effect on the material with $E/\sigma_0$=300. Although the local crack-tip constraint near the surface still increases at higher loads, the amount of increase in local constraint become progressively less obvious and the overall distribution of $A_2$ is reduced, indicating that shallow crack effect (constraint loss effect) may predominate. These comparisons based on material variations show that the biaxial effect is material dependent and more pronounced in the material with lower yield stress, which is consistent with the trend revealed in the analysis of the CR(B) specimens with straight-fronted cracks [3, 7, 18].

The trends given by the numerical analysis combined with the experimental observations in NESC-IV indicate that the biaxial loading effect in the CR(B) with a semi-elliptical crack suppresses the shallow crack effect and even increases the near-surface constraint level. The out-of-plane loading introduces a bending stress component in the beam, which results in a significant tensile stress imposed on the crack front near the surface. Therefore, at low loads, the near-surface constraint in terms of $A_2$ is enhanced while with the increasing loads the near-surface constraint is gradually controlled by the in-plane loading, showing the trend of $A_2$ become similar to that under axial loading. In addition, the constraint decreases toward the region very close to the surface (i.e. $\Phi \approx 5^o$), where the shallow crack effect predominates, regardless of the loading conditions and the loading levels.

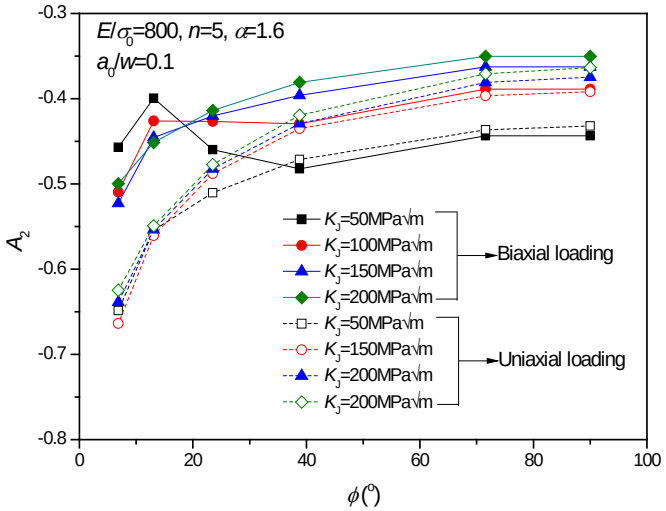


(a)

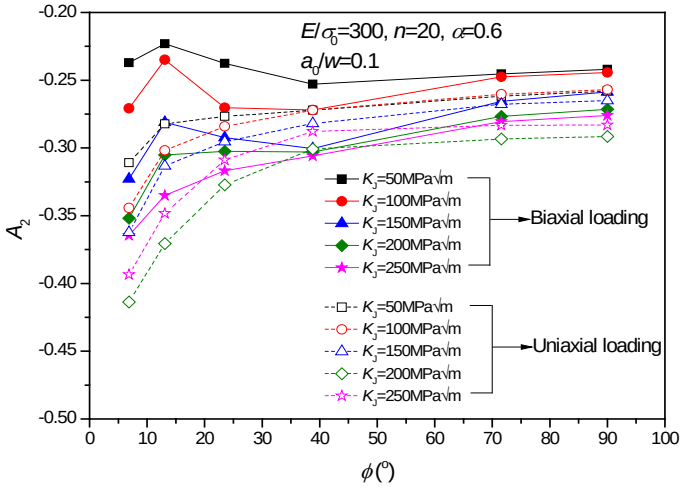


(b)

**Figure 5 Variation of $A_2$ along the crack front (the specimens with the crack depth of $a_0/W$=0.1)**

The specimens with a shallower crack ($a_0/W$=0.05) are also analyzed to assess the influence of crack depth on the biaxial effect. The variations of $A_2$ along the crack front plotted in Fig. 6 decrease slightly when compared with the curves Fig. 5, which means that the shallower crack further lowers the crack tip constraint level under both loading conditions. The local constraint increase in terms of $A_2$ at the near-surface crack front due to biaxial loading becomes more insignificant at high loads compared with that at the corresponding loads applied to the deeper crack $a_0/W$=0.1, as shown in Fig. 5. These phenomena indicate that the biaxial effect is gradually suppressed with the decreasing crack depth. When comparing results from the two materials, the $E/\sigma_0$=800 material still exhibits a more distinct biaxial effect than does the other material. The analysis above reveals that the biaxial effect is dependent on the combination of the material properties and the crack geometries. A certain crack depth with a relatively low yield strength may be more easily affected by the biaxial loading.

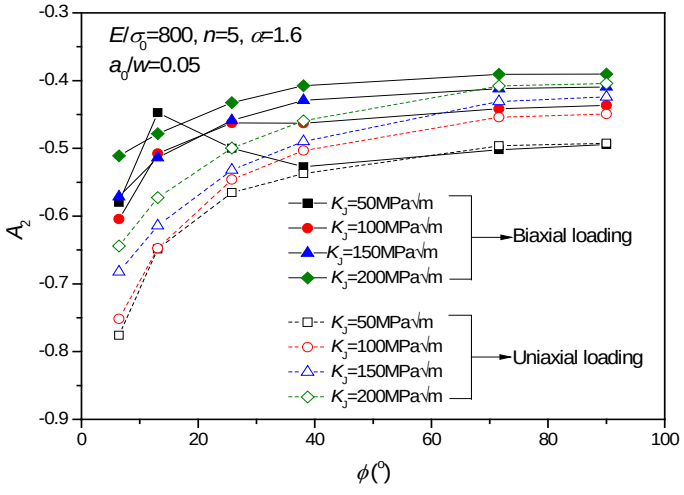


(a)

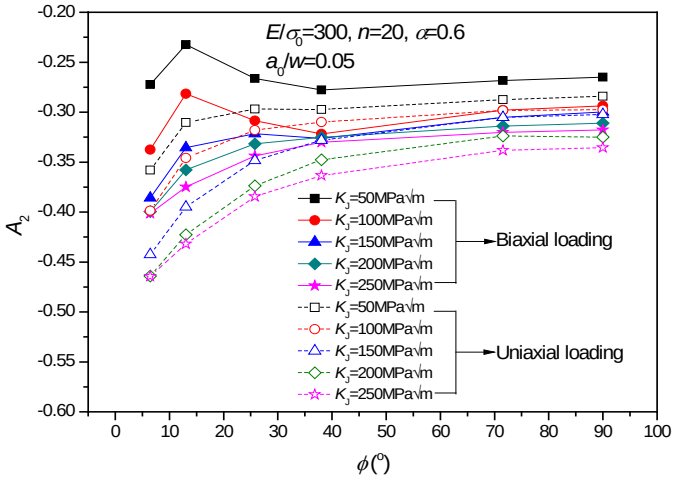


(b)

**Figure 6 Variation of $A_2$ along the crack front (the specimens with the crack depth of $a_0/W$=0.05)**

## CONCLUSIONS

Detailed FE analysis for the CR(B) specimens containing semi-elliptical cracks of different depths combined with the consideration of different material tensile properties are conducted. The variations of constraint with crack depths and material properties are quantified in terms of the $A_2$ parameter. Based on the analysis above, the conclusions can be summarized as follows:

(1) The constraint effect under biaxial loading is dependent on the tensile properties of the materials. A more pronounced biaxial effect is shown in the specimen with lower yield stress, which is consistent with the trend observed in the CR(B) specimens with straight-fronted cracks. It means that the biaxial effect on material fracture toughness may be more obvious at higher temperatures in the DBT region since the yield stress decreases with increasing temperature. Consequently, in structural integrity assessment of a surface flaw in a RPV, more attention may be given to the biaxial loading effect at a relatively higher temperature during a thermal-mechanical transient (e.g. a PTS event). In addition, when assessing the irradiation-induced fracture toughness degradation, materials exposed to low neutron fluence irradiation has lower yield stress compared to the highly irradiated condition and therefore may show greater effect due to biaxial loading.

(2) The local constraint in the near-surface region of the crack subject to biaxial loading is found to increase at low loads for the CR(B) specimens made of the lower yield strength and to increase as well at higher load levels in the case of the higher yield strength. This indicates that greater attention should be paid to the crack tip close to the surface for the assessment against cleavage fracture, especially when the yield strength of material is increased, for example, due to irradiation embrittlement or temperature drop transients.

(3) No obvious difference in the trend of constraint due to the biaxial loading is found for the crack depths studied.

## ACKNOWLEDGMENTS

Yupeng Cao and Yinbiao He would like to acknowledge the support of the Major Program of Large-Scale Advanced PWR and HTGR Nuclear Power Plant of China (2014ZX06002001).

## REFERENCES

[1] Bass, B. R., Bryson, J. W., Theiss, T. J., and Rao, M. C., 1993, "Biaxial Loading and Shallow-Flaw Effects on Crack-Tip Constraint and Fracture Toughness," USNRC Report NUREG/CR-6132, Oak Ridge National Laboratory, Oak Ridge, Tennessee, USA.

[2] Joyce, J., Link, R., and Gaies, J., 2005, "Evaluation of the Effect of Biaxial Loading on the To Reference Temperature Using a Cruciform Specimen Geometry," Journal of ASTM International, 2(1), pp. 1-18.

[3] Hohe, J., Luckow, S., Hardenacke, V., Sguaizer, Y., and Siegele, D., 2011, "Enhanced fracture assessment under biaxial external loads using small scale cruciform bending specimens," Engineering Fracture Mechanics, 78(9), pp. 1876-1894.

[4] Sharpe, L. W., and Chao, Y. J., 2013, "Constraint Effect in Fracture: Investigation of Cruciform Specimens using the J-$A_2$ Method," Procceedings of 13th International Conference on Fracture, Beijing, China, June 16-21.

[5] Taylor, N. G., Nilsson, K.-F., Minnebo, P., Bass, B. R., Swan, D. I., and Siegele, D., "An investigation of the transferability of Master Curve technology to shallow flaws in reactor pressure vessel applications," NESC-IV PROJECT, JRC, European Commission.

[6] Moinereau, D., Chapuliot, S. p., Marie, S. p., and Gilles, P., "NESC VII: A European Project for Application of WPS in RPV Assessment Including Biaxial Loading," Proceedings 2010 ASME Pressure Vessels and Piping Division Conference, Washington, USA, July 18–22, Paper No. PVP2010-25399.

[7] Cao, Y., Qian, G., He, Y., Chao, Y. J., and Niffenegger, M., 2017, "Constraint Assessment for Specimens Tested Under Uniaxial and Biaxial Loading Conditions," Proceedings 2017 ASME Pressure Vessels and Piping Division Conference, Hawaii, USA, July 16–20, Paper No. PVP2017-65979.

[8] Hutchinson, J. W., 1968, "Singular behaviour at the end of a tensile crack in a hardening material," Journal of the Mechanics and Physics of Solids, 16(1), pp. 13-31.

[9] Hutchinson, J. W., 1968, "Plastic stress and strain fields at a crack tip," Journal of the Mechanics and Physics of Solids, 16(5), pp. 337-342.

[10] Rice, J. R., and Rosengren, G. F., 1968, "Plane strain deformation near a crack tip in a power-law hardening material," Journal of the Mechanics and Physics of Solids, 16(1), pp. 1-12.

[11] ASTM E1921-16, 2016, "Standard Test Method for Determination of Reference Temperature, To, for Ferritic Steels in the Transition Range," Annual book of ASTM standards.

[12] Yang, S., Chao, Y. J., and Sutton, M. A., 1993, "Complete theoretical analysis for higher order asymptotic terms and the

HRR zone at a crack tip for Mode I and Mode II loading of a hardening material," Acta Mechanica, 98(1), pp. 79-98.
[13] Yang, S., Chao, Y. J., and Sutton, M. A., 1993, "Higher order asymptotic crack tip fields in a power-law hardening material," Engineering Fracture Mechanics, 45(1), pp. 1-20.
[14] Chao, Y. J., Yang, S., and Sutton, M. A., 1994, "On the fracture of solids characterized by one or two parameters: Theory and practice," Journal of the Mechanics and Physics of Solids, 42(4), pp. 629-647.
[15] Chao, Y. J., and Zhang, L., 1997, "Tables of plane strain crack tip fields: HRR and higher order terms."
[16] Wang, Z. X., Zhang, R. F., Chao, Y. J., and Lam, P. S., 2011, "Elastic-Plastic Constraint Analysis of Semi-Elliptic Surface Cracks in X100 Pipeline Steel," Proceedings of the ASME 2011 Pressure Vessels & Piping Division Conference, Baltimore, Maryland, USA, July 17-21, Paper No. PVP2011-57715.
[17] ABAQUS/Standard, 2011, "ABAQUS/Standard," Dassault Systèmes Simulia Corp.
[18] Bass, B. R., McAfee, W. J., Williams, P. T., and Pennell, W. E., 1999, "Fracture assessment of shallow-flaw cruciform beams tested under uniaxial and biaxial loading conditions," Nuclear Engineering and Design, 188(3), pp. 259-288.